THE JOURNAL OF PHYSICAL CHEMISTRY A

Article

pubs.acs.org/JPCA

Bimolecular Encounters and Re-Encounters (Cage Effect) of a Spin-Labeled Analogue of Cholestane in a Series of *n*-Alkanes: Effect of Anisotropic Exchange Integral

Andrew D. Vandenberg,[†] Barney L. Bales,[†] K. M. Salikhov,[‡] and Miroslav Peric*[,†]

[†]Department of Physics and Astronomy and The Center for Supramolecular Studies, California State University at Northridge, Northridge, California 91330, United States

[‡]Zavoisky Physical-Technical Institute, Russian Academy of Sciences, Sibirsky trakt 10/7, Kazan 420029, Russian Federation

ABSTRACT: Electron paramagnetic resonance (EPR) spectra of the nitroxide spin probe 3β-doxyl-5α-cholestane (CSL) are studied as functions of the molar concentration, c, and the temperature, T, in a series of *n*-alkanes. The results are compared with a similar study of a much smaller spin probe, perdeuterated 2,2,6,6-tetramethyl-4-oxopiperidine-1-oxyl (pDT). The Heisenberg spin exchange (HSE) rate constants, K_{ex}, of CSL are similar in hexane, octane, and decane and are about one-half of those for pDT in the same solvents. They are also about one-half of the Stokes−Einstein−Perrin prediction. This reduction in HSE efficiency is attributed to an effective steric factor, f_{eff}, which was evaluated by comparing the results with the Stokes−Einstein−Perrin prediction or with pDT, and it is equal to 0.49 ± 0.03, independent of temperature. The unpaired spin density in CSL is localized near one end of the long molecule, so the exchange integral, J, leading to HSE, is expected to be large in some collisions and small in others; thus, J is modeled by an ideal distribution of values of $J = J_0$ with probability f and $J = 0$ with probability $(1 - f)$. Because of rotational and translation diffusion during contact and between re-encounters of the probe, the effective steric factor is predicted to be $f_{eff} = f^{1/2}$. Estimating the fraction of the surface of CSL with rich spin density yields a theoretical estimate of $f_{eff} = 0.59 \pm 0.08$, in satisfactory agreement with experiment. HSE is well described by simple hydrodynamic theory, with only a small dependence on solvent−probe relative sizes at the same value of T/η, where η is the viscosity of the solvent. This result is probably due to a fortuitous interplay between long- and short-range effects that describe diffusion processes over relatively large distances. In contrast, dipole−dipole interactions (DD) as measured by the line broadening, B_{dip}, and the mean time between re-encounters within the cage, τ_{RE}, vary significantly with the solvent−probe size ratio at the same value of T/η. For these phenomena, dominated by short-range diffusion, the reciprocal fractional free volume V_0/V_f provides a better description of the diffusion. Thus, B_{dip} and τ_{RE} form common curves when plotted vs V_0/V_f. As a result, the fractional broadening by DD occurs at an order of magnitude higher values of T/η for CSL compared with pDT.

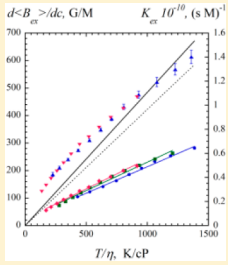

1. INTRODUCTION

For more than five decades, Heisenberg spin exchange (HSE) has been used to study bimolecular collisions of nitroxide spin probes (nitroxides) in solutions.[1−10] For a list of acronyms, see Table 1. The textbook relationship between the HSE rate constant, K_{ex}, and the rate constant of collisions, K_D, is as follows:

Table 1. Abbreviations and Acronyms

DD	dipole−dipole interactions
HSE	Heisenberg spin exchange
pDT	perdeuterated 2,2,6,6-tetramethyl-4-oxopiperidine-1-oxyl spin probe
CSL	3β-doxyl-5α-cholestane spin probe
EPR	electron paramagnetic resonance

$$K_{ex} = p f_{eff} K_D \quad (1)$$

where the efficiency, p, is given by

$$p = \frac{1}{2}\frac{J_0^2 \tau_c^2}{1 + J_0^2 \tau_c^2} \quad (2)$$

where J_0 is the exchange integral and τ_c the duration of the contact.[1] The effective steric factor f_{eff} was introduced[1] to account for the fact that J_0 can depend on the relative orientation of the two nitroxides during contact but has evolved to include other effects that hinder spin exchange; for example, the structure of the radical, solvation of the NO group, etc.[1]

According to eqs 1 and 2, a measurement of K_{ex} is sufficient to determine K_D provided that f_{eff} and the product $J_0\tau_c$ are known. The behavior of the electron paramagnetic resonance (EPR) spectra is different for HSE that is strong ($J^2\tau_c^2 \gg 1$), intermediate ($J^2\tau_c^2 \approx 1$), or weak ($J^2\tau_c^2 \ll 1$). Fortunately, except for solutions of very low viscosity, HSE between small nitroxides to date has been found to be strong, which greatly simplifies the analysis and does not require a knowledge of J_0. We mean by *small* that the unpaired electron wave function extends over a significant portion of the nitroxide. See the arguments on p 180 of ref 1 and on p 1409 of ref 6 that strong exchange is expected for free radicals.

Received: October 17, 2012
Revised: November 27, 2012
Published: November 29, 2012

For strong exchange, eq 1 becomes

$$K_{ex} = \frac{1}{2} f_{eff} K_D \tag{3}$$

Approximating the diffusion rate constant by combining the Stokes−Einstein equation with the Smoluchowski equation, yields the Stokes−Einstein−Smoluchowski equation

$$K_{ex} = \frac{1}{2} f_{eff} \frac{8 k_B T}{3\eta} \tag{4}$$

where k_B is the Boltzmann constant and η the shear viscosity.[1] Note that, due to the factor f_{eff}, the magnitude of K_{ex} is not an indicator of strong HSE; rather, the linearity of K_{ex} with T/η confirms strong HSE.

In this work, we study the large nitroxide 3β-doxyl-5α-cholestane (CSL) (Scheme 1) in a series of *n*-alkanes. The

Scheme 1. 3β-Doxyl-5α-cholestane (CSL) and Perdeuterated 2,2,6,6-Tetramethyl-4-oxopiperidine-1-oxyl (pDT); the Active Portion of CSL Is Shown to the Left of the Dashed Line

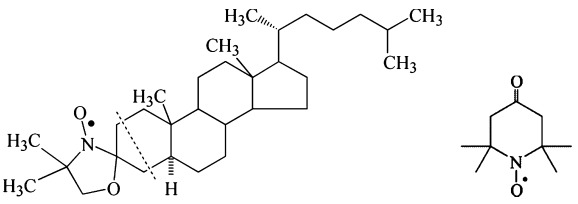

unpaired spin density in CSL is localized near one end of the long molecule, so the exchange integral, *J*, leading to HSE is expected to be large in some collisions and small in others. We adopt a simplified distribution of the exchange integral as follows:

$$w(J) = f \cdot \delta(J - J_0) + (1 - f) \cdot \delta(J) \tag{5}$$

The fact that the spin density of the unpaired electron is localized at one end of the long molecule makes eq 5 plausible. The active region of CSL is shown to the left of the dashed line in Scheme 1.

The Stokes−Einstein equation requires a spherical probe molecule that is larger than the solvent molecules. Because the shape of CSL is more ellipsoidal than spherical, the value of K_D may be corrected by a method due to Perrin[11] who derived an analytical expression for the diffusion of a prolate ellipsoid of revolution. Evaluating the ratio of the diffusion coefficients for a sphere and a prolate ellipsoid of the same volume yields the following:

$$f_{Perrin} = \rho^{2/3} \frac{1}{2\sqrt{1 - \rho^2}} \times \ln \frac{1 + \sqrt{1 - \rho^2}}{1 - \sqrt{1 - \rho^2}} \tag{6}$$

with $\rho = R_E/R_P$ where R_E is the equatorial axis and R_P is the axis of revolution or polar axis of the ellipsoid; note that as ρ goes to 1, the limit of eq 6 is 1. Thus, eq 4 becomes

$$K_{ex} = f_{eff} \frac{4 k_B T}{3\eta} f_{Perrin} \tag{7}$$

where the correction f_{Perrin} is discussed below. We call eq 7 the Stokes−Einstein−Perrin equation.

The present experiment is now feasible due to recent advances in separating the effects of HSE and those of the dipole−dipole interaction (DD).[12] Both interactions contribute to the line width. They both lead to dispersion and line shifts but with opposite sign for DD and HSE.[13,14] Using nonlinear least-squares EPR spectral fitting[15] and the recent comprehensive theoretical treatment of the effects of HSE and DD interactions on EPR spectra of nitroxides in solution,[14] we have recently been able to separate the two contributions.[12]

The present work complements a study of bimolecular collisions of the smaller, more nearly spherical nitroxide, perdeuterated 2,2,6,6-tetramethyl-4-oxopiperidine-1-oxyl (pDT), in a series of *n*-alkanes.[16] Each bimolecular collision of a nitroxide pair was separated into an encounter followed by a series of re-encounters. For pDT, the HSE rate constant as a function of T/η formed a common curve for hexane, decane, and hexadecane. This appears to indicate that the HSE rate constant is dominated by hydrodynamic forces. Since the size of pDT is comparable to the size of the *n*-alkanes used, this close coincidence of the measured HSE rate constant with the Stokes−Einstein prediction is very likely due to a near cancellation of terms in the diffusion coefficient.[17] In contrast, the re-encounter rate depended on the relative sizes of probe and solvent and departed from the Stokes−Einstein prediction. The re-encounter rates are well correlated with the free volume available in the solvent and the isothermal compressibility, that is, the re-encounter rates form a common curve when plotted versus either the free volume or the compressibility.

The purpose of the work is 2-fold: (1) to compare the results of CSL with pDT and (2) to focus on contributions to f_{eff} due to an anisotropic exchange integral.

2. THEORY

2.1. Separating HSE and DD. The method has been published in detail in ref 12; only the major features will be presented.

K_{ex} can be found from the concentration dependence of the HSE broadening, B_{ex}, as follows

$$K_{ex} = \frac{3\sqrt{3}\gamma}{4} \frac{dB_{ex}}{dc} \tag{8}$$

where c (mol/L) is the concentration and γ is the gyromagnetic ratio of the electron. The broadening of the M_j line may be extracted from the peak-to-peak EPR line width as follows:

$$B(M_j) = \Delta H^L_{pp}(c)_{M_j} - \Delta H^L_{pp}(0)_{M_j} = B_{ex}(M_j) + B_{dip}(M_j) \tag{9}$$

where $\Delta H^L_{pp}(c)_{M_j}$ is the Lorentzian line width at concentration c broadened by HSE and/or DD, $\Delta H^L_{pp}(0)_{M_j}$ is the Lorentzian line width in the absence of these interactions, and B_{dip} is the DD broadening. Both DD and HSE contribute to a dispersion component of the line shape but with opposite signs.[13,14] The value of the normalized dispersion height, $(V_{disp}/V_{pp})^{\#}$, corrected for instrumental dispersion and for a nonlinear dependence on the broadening[18] is proportional to c; thus, a plot of $(V_{disp}/V_{pp})^{\#}$ vs $\langle B\rangle/A_0$,where V_{pp} is the peak-to-peak height of the line, A_0 is the hyperfine spacing at $c = 0$, and $\langle B\rangle$ is the value of $B(M_j)$ averaged over the three lines is expected to yield a straight line passing through the origin as follows:

$$\left(\frac{V_{disp}}{V_{pp}}\right)^{\#} = k \frac{\langle B\rangle}{A_0} \tag{10}$$

dx.doi.org/10.1021/jp310297d | J. Phys. Chem. A 2012, 116, 12460−12469

The ratio of the broadening by HSE to the overall broadening, Ω, is calculated[12] from the slope of the line k, which may be positive (HSE dominates) or negative (DD dominates)

$$\Omega = \frac{\langle B_{ex}\rangle}{\langle B\rangle} = \frac{k + 2b}{1 + 2b} \tag{11}$$

where b depends on the details of the molecular diffusion;[14] however, we demonstrated in ref 12, using the permanent diffusion model,[14] that taking b to be constant, $b = 1/4.75$, gives a negligible error in the separation of DD and HSE. The required values of B_{ex} are computed from eq 11.

Note that the Lorentzian line widths, heights, and positions as well as $(V_{disp}/V_{pp})^{\#}$ are obtained by nonlinear least-squares spectral fitting as detailed in recent publications.[12,19−23] A concise detailed description of the EPR parameter extraction from the EPR spectra by spectral fitting is given in Tables 1 and 2 of ref 19.

2.2. Mean Time between Re-Encounters. The positions of EPR lines are affected by coherence transfer induced by both DD and HSE, which shift the resonance frequency of the outer absorption EPR lines, producing a hyperfine spacing, A_{abs}, that is defined to be one-half of the difference in the low- and high-field resonance fields. This shift is quadratic with $\langle B\rangle/A_0$. In addition, the lines are shifted linearly with $B_{ex}/A_0 = \Omega\,\langle B\rangle/A_0$ due to spin precession during the time τ_c and during the mean time between re-encounters, τ_{RE}.[12,14,23] Combining the two effects

$$\frac{A_{abs}}{A_0} = 1 - \kappa_{ER}\Omega\frac{\langle B\rangle}{A_0} - \frac{9}{32}\left(\frac{k\langle B\rangle}{A_0}\right)^2 \tag{12}$$

where, for strong exchange and $f_{eff} = 1$,

$$\kappa_{ER} = \frac{3\sqrt{3}}{8}\left[\gamma A_0\tau_c + \frac{1}{3}(1 + \sqrt{2})\sqrt{\gamma A_0\tau_{RE}/2}\right] \tag{13}$$

In cases in which spin exchange does not occur upon every collision, then, in eq 13, τ_{RE} would be replaced by τ_{RE}^{HSE}, defined to be the mean time between collisions that result in spin exchange. Usually, τ_c is much less than τ_{RE}, so the first term in the brackets may be neglected.

$$\kappa_{ER} = \frac{\sqrt{3}}{8}(1 + \sqrt{2})\sqrt{\gamma A_0\tau_{RE}^{HSE}/2} \tag{14}$$

The relationship between τ_{RE}^{HSE} and τ_{RE} depends on the details of rotations and translations between re-encounters. If we assume that the same effective spin exchange rate holds throughout a given encounter, then we may tentatively write

$$f_{eff}\,\tau_{RE}^{HSE} = \tau_{RE} \tag{15}$$

According to the continuous diffusion model[24] and the Stokes−Einstein approximation, the re-encounter time is given by[16]

$$\tau_{RE} = \frac{3\pi r_0^3}{2k_B}\frac{\eta}{T} \tag{16}$$

where r_0 is the distance of bimolecular approach. Usually the closest approach radius, r_0, is estimated as the sum of van der Waals radii of colliding partners. In the case of CSL, $r_0 = 9.9$ Å, and for pDT, $r_0 = 7.0$ Å .

2.3. Free Volume and Diffusion. According to Doolittle, the viscosity of alkanes can be accurately described as an exponential function of their fractional free volumes.[25] The diffusion constant in a liquid can also be described by the same functional dependence[16,26]

$$D = A_{FV}\,e^{-B(V_0/V_f)} \tag{17}$$

where A_{FV} and B are constants for a given probe−solvent system. V_f and V_0 are the total compressible free volume in a liquid and volume of the sample at 0 K, respectively; $V_f = V - V_0$, where V is the volume of the sample at T. $B = \gamma(v^*)/(V_0)$, where γ $(0.5 \le \gamma \le 1)$ is a factor introduced to account for overlap of free volume, and v^* is the volume of a critical free void necessary for diffusion. We call eq 17 the Doolittle−Cohen−Turnbull equation.

2.4. Effect of an Anisotropic Exchange Integral. In general, the HSE rate constant, K_{ex}, can be presented as

$$K_{ex} = 4\pi\sigma_{ex}D \tag{18}$$

where D is the mutual diffusion coefficient of two colliding partners, and σ_{ex} is an effective spin exchange radius. This radius was calculated for two models of the inter-radical distance dependence of the exchange interaction.[1,27,28]

One model suggests that the exchange integral equals J_0 in a narrow interaction spherical layer of width Δ, that is $J(r) = J_0$ when $r_0 \le r \le r_0 + \Delta$ and $J(r) = 0$ outside of this layer. For this model, the effective exchange radius is given as[1]

$$\sigma_{ex} = pr_0 \tag{19}$$

where the exchange efficiency, p, is given by eq 2 with

$$\tau_c = \frac{r_0\Delta}{D} \tag{20}$$

Note that, for this model, the maximum effective exchange radius equals

$$\sigma_{ex} = \frac{r_0}{2} \tag{21}$$

Another model suggests that the exchange integral decreases exponentially when two radicals separate, i.e.,

$$J(r) = J_0\,e^{-(r-r_0)/r_e} \tag{22}$$

where r_e describes the decrement of the exchange integral. As a reasonable estimate, one can use $r_e = 0.03$ nm. For this model, the effective exchange radius is given by[1,28]

$$\sigma_{ex} = \mathrm{Re}\left\{\frac{r_0}{2} + r_e\left[C + \ln\left(\frac{r_0}{2}\right) - \frac{C_1}{2}\right]\right\} \tag{23}$$

where $z_0 \equiv 2(iJ_0r_e^2/D)^{1/2}$; C-Euler number, $C_1 = \pi\{(N_1(z_0)z_0r_0 - 2N_0(z_0)r_e)/(J_1(z_0)z_0r_0 - 2J_0(z_0)r_e)\}$; and J_n and N_n are Bessel functions of the first and second kind, respectively. When the diffusion coefficient decreases, two colliding partners can succeed to exchange spin states even at relatively large distance between them because, due to a slow diffusion, the particles spend more time in an interaction region. As a result, the effective radius of spin exchange is expected to increase when diffusion coefficient decreases. For example, when the diffusion coefficient decreases, the effective time two particles spend in a layer with a thickness r_e increases as $\tau = r_e^2/D$. It follows from eq 23 that, in the limit of strong exchange, the effective exchange radius is determined by this characteristic time (see eq 1.247 of ref 1)

$$\sigma_e = \frac{1}{2}[r_0 + r_e\ln(|J_0|\tau)] = \frac{1}{2}[r_0 + r_e\ln(|J_0|r_e^2/D)] \tag{24}$$

Figure 1 presents a typical dependence of the exchange radius σ_{ex}, eq 23, on the diffusion coefficient D for CSL ($r_0 = 9.9$ Å) and pDT ($r_0 = 7.0$ Å) with $J_0 = 10^{12}$ rad/s and $r_e = 0.3$ Å, while D changes in an interval $\{10^{-6}$−10^{-5} cm^2/s$\}$. Note that $D = 10^{-5}$ cm^2/s corresponds to the self-diffusion coefficient in water around room temperature.

dx.doi.org/10.1021/jp310297d | J. Phys. Chem. A 2012, 116, 12460−12469

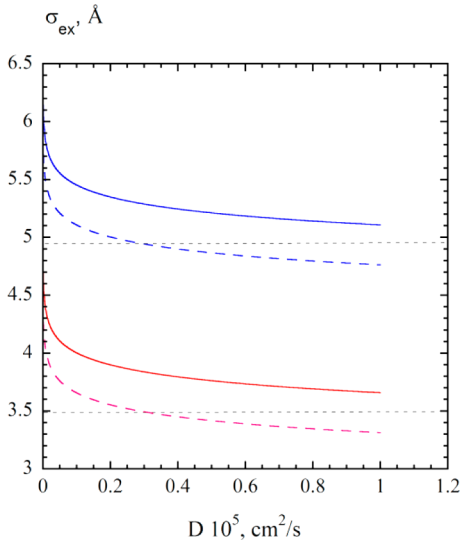

Figure 1. Exchange radius σ_{ex}, eq 23, versus the diffusion coefficient D. Equation 23 is evaluated assuming $r_0 = 9.9$ Å (blue, CSL) and 7.0 Å (red, pDT), $r_e = 0.3$ Å, $J_0 = 10^{12}$ rad/s (solid lines), and $J_0 = 10^{11}$ rad/s (dashed lines).

Parameters chosen in Figure 1 correspond to a strong exchange limit. In the framework of the first model, eqs 18−20, in the strong exchange limit the effective exchange radii are expected to be $\sigma_{ex} = r_0/2 = 4.95$ and 3.5 Å for CSL and pDT, respectively. However, for the case considered in eq 23, the exchange radii exceed these values (see the solid lines in Figure 1) since the exchange interaction operates not only at the closest approach of two colliding radicals. From Figure 1, one can see that the effective exchange radius can exceed $\sigma_{ex} = r_0/2$ by about 10%.

Figure 1 shows that the effective exchange radius increases when the diffusion coefficient decreases. For the parameters chosen, which correspond to a strong exchange limit for the closest approach of colliding radicals, the effective exchange radius is always larger than one given by eq 21. This occurs due to an increase of the average time spent by colliding partners in the interaction region $r > r_0$.

If the exchange integral at the closest approach equals 10^{11} rad/s, then the D dependence of the exchange radii are given by the dashed lines in Figure 1. In the case of strong exchange when $J_0 r_0 r_e/D > 1$, the effective spin exchange radius is expected to be around

$$\sigma_{ex} = \frac{r_0 + 2r_e}{2} \approx \frac{r_0}{2} \tag{25}$$

Thus, the closest approach collisions give the major contribution to the spin exchange at reasonable values of parameters. In our estimates below, we will use this value of the effective exchange radius.

The exchange radii can be less than one given by eqs 22−24 due to an anisotropic distribution of the electron spin density. This leads to a steric effect in the spin exchange. Consider the simple model, eq 5, to take into account the fact that J_0 can depend on the relative orientation of the two nitroxides during contact. At first glance, it seems that this distribution would lead to eq 3 or 4 with $f_{eff} = f$, which would be true if the spin exchange act were instantaneous and there were no re-encounters.

However, the situation is more complicated because of two processes: rotational diffusion of colliding partners[27] and translational diffusion between re-encounters of radicals.[29] Both of these processes change the mutual orientation of two colliding radicals; they tend to average the anisotropic effect of the spin exchange. If the rotational diffusion of radicals were fast enough to average the exchange interaction during a collision, then the efficiency of the spin exchange would be given by eq 2 with J_0 replaced by fJ_0. This is unlikely because $\tau_c \approx 10^{-13}$ s, while rotational correlation times are of order of 10^{-11} s or more; the shortest rotational correlation time is about 3×10^{-11} s for CSL in hexane at 323 K, and $\eta = 0.237$ cP.

The effect of the translational diffusion on a steric factor was considered in ref 29. It was shown that, for this mechanism of averaging of the spin exchange anisotropy, the effective steric factor appears as $f^{1/2}$. This very nonlinear dependence of the effective steric factor f_{eff} on the geometric factor f arises from the peculiar statistics of re-encounters of the two colliding paramagnetic molecules. The probability that two partners will re-encounter in an interval of time $(t, t + dt)$ was studied first in ref 30. In the case of permanent diffusion model, this probability equals $w(t)dt = mt^{-3/2} \exp(-\pi m^2/(p^2 t))dt$. Here, the distribution parameters m and the full re-encounter probability p are determined by molecular kinetic parameters: the distance of closest approach r_0 and the jump length of the partners in an individual diffusion step. This distribution differs from the simple Poisson distribution. Manifestation of both rotational and translational diffusion in the spin exchange rate was numerically studied in ref 31. When both rotational and translational diffusions are involved, the effective steric factor is

$$f^{1/2} \le f_{eff} \le 1 \tag{26}$$

2.5. Estimate of the Value of *f* for CSL. Let S_{active} and S_{CSL} be the surface areas of the active region with rich spin density and the entire molecule, respectively. Upon collision, the probability that the active region of one CSL collides with the active region of the second is as follows:

$$f = (S_{active}/S_{CSL})^2 \tag{27}$$

The unpaired spin density is localized in the region of the doxyl ring. The spin density is unknown for CSL; however, for doxyl-labeled *n*-alkanes, EPR and NMR have shown[32] that considerable spin density resides on the methyl group adjacent to the attachment point of the doxyl ring. The same is true of doxylcyclohexane.[33] As a first-order estimate, we assume that the active region comprises the doxyl plus 2 methylene groups shown to the left of the dashed line in Scheme 1. We estimate the uncertainty by adding or subtracting 2 methylene groups.

Taking the active region to be approximately spherical yields

$$S_{active} = (36\pi)^{1/3}(V_{active})^{2/3} \tag{28}$$

Taking CSL to be a prolate ellipsoid with minor and major axes given by R_E and R_P, respectively, yields

$$S_{CSL} = g(\rho)(V_{CSL})^{2/3} \tag{29}$$

with

$$g(\rho) = \frac{2\pi\rho^2\left(1 + \frac{1}{\rho(\sqrt{1-\rho^2})}\sin^{-1}(\sqrt{1-\rho^2})\right)}{\left(\frac{4}{3}\pi\rho^2\right)^{2/3}} \tag{30}$$

where $\rho = R_E/R_P$ (eq 6), with $\rho = 1/3.5$ and $g(\rho) = 6.0$. Dividing eq 28 by eq 29 yields

$$(S_{active}/S_{CSL}) = 1.2(V_{active}/V_{CSL})^{2/3} \tag{31}$$

dx.doi.org/10.1021/jp310297d | J. Phys. Chem. A 2012, 116, 12460−12469

Using the lower limit of eq 26, we obtain

$$f_{\text{eff}} = (f)^{1/2} = (S_{\text{active}}/S_{\text{CSL}}) \quad (32)$$

The pertinent volumes are computed using the method of Bondi.[34,35] The volume of the doxyl ring is 142 Å^3 and that of 2 methyl groups is 35 Å^3. Therefore, V_{active} = 177 ± 35 Å^3. The volume of CSL is V_{CSL} = 511 Å^3. Substituting into eq 32 gives f_{eff} = 0.59 ± 0.08. Considering the active region to be a sphere likely overestimates the value $(S_{\text{active}}/S_{\text{CSL}})$. If we assume the other extreme where the shapes of the active group and CSL are taken to be the same, f_{eff} = 0.49 ± 0.07.

3. MATERIALS AND METHODS

3β-Doxyl-5α-cholestane, Scheme 1, (CSL; lot no. 100H37091) purchased from Aldrich Chemical Co. was dissolved in the following three solvents: 99+% *n*-hexane from MCB Reagents and 99+% *n*-octane and 99+% *n*-decane both from Sigma-Aldrich. For each of the three solvents, a stock solution was prepared at a concentration near 30 mM, close to the saturation point. Lower concentrations were prepared by dilution by weight to form 10 concentrations of CSL in each solvent in the range 0.3−30 mM. Samples were extracted from each solution into disposable polytetrafluoroethylene (PTFE) capillary tubing produced by Zeus. Each tube was folded in half to form a vee, sealed with hot pliers,[16] and inserted into a quartz tube (manufactured by Wilmad Glass company) with a hole in the bottom to allow for nitrogen equilibration of the sample in the EPR cavity. The quartz tube was placed into the cavity of a Bruker ESP 300E spectrometer equipped with a Bruker variable temperature unit (Model B-VT-2000). This way, the nitrogen that was used to control the temperature replaced the oxygen in the sample reducing the broadening of the EPR lines caused by molecular oxygen.[36] All samples were deoxygenated until no further reduction of the line width was observed (approximately 60 min) before beginning a run.

EPR spectra were obtained for each sample at 9.39 GHz using a sweep width of 60 G at a center field of 3308 G, modulation frequency of 100 kHz, and modulation amplitude of 1.0 G. Values of *c* are accurate to about 2% and the relative concentrations precise to within 0.1%. Five EPR spectra, one after the other, were taken of each sample at 10 different temperatures with intervals of 10 K between each. Care was taken to keep the temperature in a range at least 20 K from the freezing or boiling points of the solvents used. The temperature of each sample was monitored with a thermocouple manufactured by Bailey Instruments. Measurement temperatures were maintained constant within ±0.2 K.

4. RESULTS

Figure 2 shows representative EPR spectra and fits of 0.25 mM and 7.5 mM CSL in hexane at 323 K. These spectra are similar to those in our previous papers.[16,19,20,22,37] The only difference is that the lowest concentration spectrum shows incipient resolution due to hyperfine interactions with protons, Figure 2a. With a reduced modulation amplitude, it is possible to partially resolve each nitrogen line into proton hyperfine lines. We intentionally used a modulation of 1.0 G to produce an inhomogenously broadened line of each manifold, exploiting the fact that the modulation broadening contributes only to the Gaussian component of the ESR line.[38,39] For the three lines in Figure 2a, the values of the ratio of the Gaussian to Lorentzian line width, $\chi = \Delta H^{\text{G}}_{\text{pp}}/\Delta H^{\text{L}}_{\text{pp}}$,[40] are 4.42 ± 0.03, 4.39 ± 0.04, and 4.01 ± 0.03.

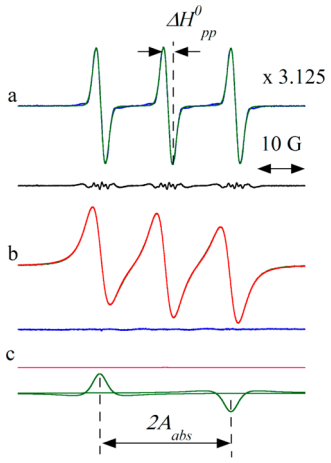

Figure 2. EPR spectra and their fits at 323 K of (a) 0.25 and (b) 7.5 mM CSL in hexane; below each spectrum is the residual; i.e., the difference in the spectra and the fits. The nonlinear least-squares fit is indistinguishable from the spectrum in panel b. In panel a, the fit is noticeably different from the spectrum in the wings of each line due to ^{13}C lines. The residual in panel a shows clearly ^{13}C lines, as well as incipient resolution due to unresolved proton manifolds. This kind of residual was only observed for the lowest two concentrations in all three *n*-alkanes. At the higher concentrations, the residual was as in panel b. The top trace in panel c is the central dispersion line showing negligible dispersion, indicative of a well-balanced microwave bridge, while the lower two traces are the low- and high-field dispersion lines of the spectrum from panel b.

Utilizing these values, the Lorentzian component of the line width, $\Delta H^{\text{L}}_{\text{pp}}$, is computed as detailed in ref 40. Plots of $\Delta H^{\text{L}}_{\text{pp}}$ vs *c* are linear with coefficients of correlation as follows: *r* = 0.996 for hexane; 0.998 for octane; and 0.999 for decane. From intercepts of linear fits, we obtain $\Delta H^{\text{L}}_{\text{pp}}(0)$. Values of B_{j} were computed from eq 9 and averaged over the three lines to give values of $\langle B \rangle$. Figure 3 shows typical values vs *c* in hexane at 243 K (squares), octane at 303 K (circles), and decane at 363 K (diamonds).

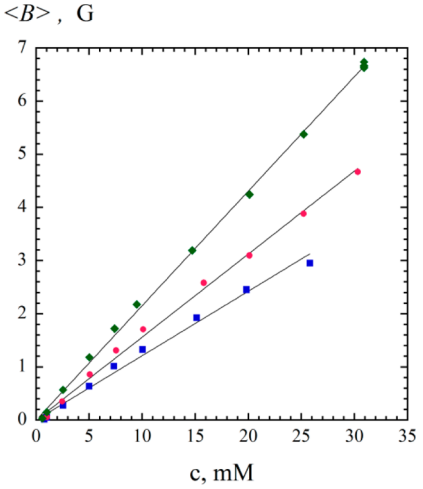

Figure 3. Total broadening versus CSL concentration in hexane at 243 K (squares), octane at 303 K (circles), and decane at 363 K (diamonds). The solid lines are linear least-squares fits to the origin. Coefficients of correlation are 0.996 for hexane, 0.998 for octane, and 0.999 for decane.

Figure 4 displays plots of $(V_{\text{disp}}/V_{\text{pp}})^{\#}$, which are averages of the values for the lower and upper EPR lines, as functions of $\langle B \rangle/A_0$. These data are fit to eq 10 to find the values of *k*, which

dx.doi.org/10.1021/jp310297d | J. Phys. Chem. A 2012, 116, 12460−12469

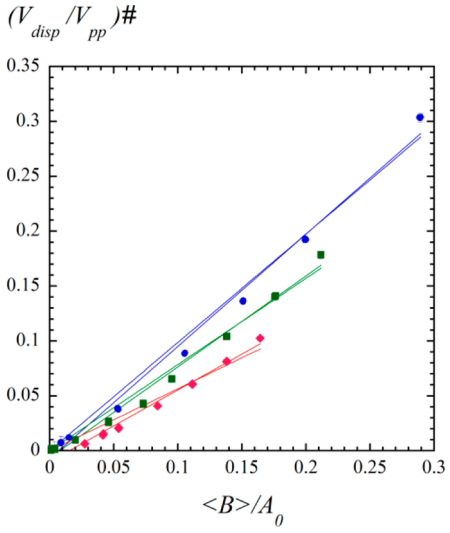

Figure 4. Values of $(V_{disp}/V_{pp})^{\#}$ versus the total normalized broadening for CSL in hexane at 323 K (circles) and 243 K (squares) and decane at 263 K (diamonds). The solid lines are linear least-squares fits with and without intercept. All correlation coefficients are greater than 0.99 except the linear least-squares fit to the origin for CSL in decane at 263 K (diamonds), which is 0.978.

were substituted into eq 11 to calculate the values of Ω shown in Figure 5. The uncertainties are one-half the difference in the

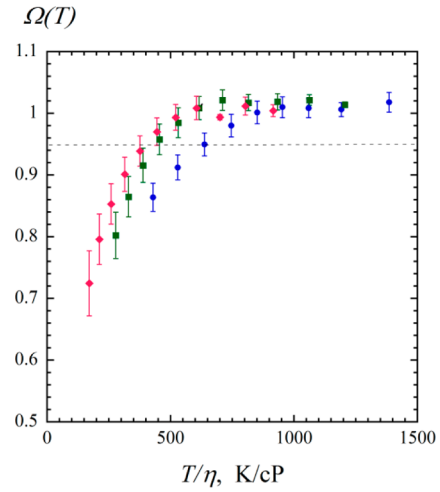

Figure 5. Fractional broadening by HSE of CSL versus T/η in hexane (circles), octane (squares), and decane (diamonds). The dashed line is Ω = 0.95.

slopes of the linear fit constrained to the origin and without this constraint. To facilitate the discussion, we adopt the convention that DD becomes significant at $\Omega \leq 0.95$.[12] Figure 5 shows that DD in hexane starts at T/η = 640 K/cP (η = 0.41 cP at 263 K), in octane at T/η = 450 K/cP (η = 0.63 cP at 282 K), and in decane at T/η = 400 K/cP (η = 0.77 cP at 306 K). In the case of pDT in the same solvents, DD interactions are negligible.[16] In contemplating the data in Figure 5, one needs to bear in mind that part of the decrease in Ω with decreasing temperature is due to the fact that the broadening by HSE is decreased by a factor of $f_{eff} < 1$.

To gain insight into how the details of the solvent affect the fractional broadening, Figure 6 shows plots of Ω vs V_0/V_f

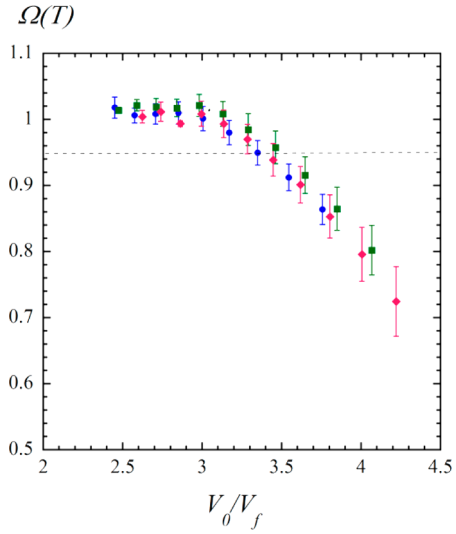

Figure 6. Fractional broadening by HSE of CSL versus V_0/V_f in hexane (circles), octane (squares), and decane (diamonds). The dashed line is Ω = 0.95.

calculated from the Doolittle equation[25] as detailed in ref 16. Figure 6 shows that DD becomes significant at V_0/V_f = 3.40 ± 0.06 for all three solvents.

Figure 7 shows plots of $d\langle B_{ex}\rangle/dc = \Omega d\langle B\rangle/dc$ vs T/η for CSL in all three solvents together with the hydrodynamic predictions,

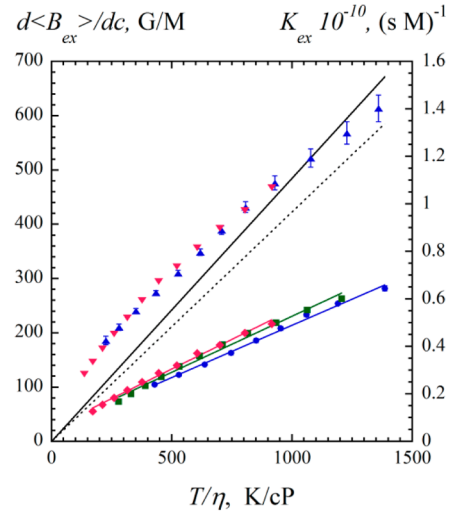

Figure 7. HSE broadening constant of CSL versus T/η in hexane (circles), octane (squares) and decane (diamonds) and of pDT in hexane (triangles) and decane (inverted triangles).[16] The solid lines through the CSL data are linear fits. The solid line is the Stokes–Einstein–Smoluchowski prediction and the dashed line is the Stokes–Einstein-Perrin prediction for a prolate ellipsoid, eq 7. The right-hand ordinate is the HSE rate constant, eq 8.

eqs 4 and 7. The right-hand ordinate is the HSE rate constant, eq 8. For comparison, the results for pDT in hexane and decane from ref 16 are also given. The solid line is the Stokes–Einstein–Smoluchowski equation, while the dashed line is the Stokes–Einstein–Perrin prediction assuming ρ = 1/3.5 ($1/f_{Perrin}$ = 1.15). In the case of pDT, the HSE rate constant is similar to the Stokes–Einstein–Smoluchowski prediction, whereas the HSE rate constant of CSL in *n*-alkanes is well below the Stokes–Einstein–Perrin prediction. However, in both cases, the data from all solvents

dx.doi.org/10.1021/jp310297d | J. Phys. Chem. A 2012, 116, 12460–12469

are close to each other indicating that the particulars of solvent structure and dynamics are not very important determinants of K_{ex}.

We analyze the data in Figure 7 under the assumptions leading to eq 7. The linearity of the data above $T/\eta = 200$ K/cP strongly suggests that both CSL and pDT undergo strong exchange, thus reinforcing theoretic expectations; for example, on p 180 of ref 1 and on p 1409 of ref 6.

There are two reasonable methods to evaluate the steric factor, f_{eff}: (1) compute f_{eff} assuming that K_D is given by the Stokes−Einstein−Perrin relationship or (2) adopt pDT as a benchmark probe and assume that $f_{eff} = 1$.

For method 1, we divide slopes of the straight lines through the CSL data in Figure 7 by that of the Stokes−Einstein−Perrin prediction. This yields $f_{eff} = 0.46$, 0.49, and 0.52 for hexane, octane, and decane, respectively. Averaging over the three solvents yields $f = 0.49 \pm 0.03$.

To proceed with method 2, we observe that

$$K_{ex}(\mathrm{CSL}) = \frac{1}{2} f_{eff} K_D(\mathrm{CSL}) \tag{33}$$

and

$$K_{ex}(\mathrm{pDT}) = \frac{1}{2} K_D(\mathrm{pDT}) \tag{34}$$

The collision rate constants, according to the Perrin method are related by $K_D(\mathrm{CSL}) = f_{\mathrm{Perrin}} K_D(\mathrm{pDT})$. Thus, the steric factor becomes, dividing eq 33 by eq 34 and utilizing eq 8

$$f_{eff} = \frac{1}{f_{\mathrm{Perrin}}} \frac{K_{ex}(\mathrm{CSL})}{K_{ex}(\mathrm{pDT})} = 1.15 \frac{dB_{ex}/dc(\mathrm{CSL})}{dB_{ex}/dc(\mathrm{pDT})} \tag{35}$$

Dividing the results in Figure 7 for CSL by those for pDT and multiplying by 1.15 yields $f_{eff} = 0.48 \pm 0.03$ in hexane and 0.49 ± 0.03 in decane. The results from both solvents are independent of temperature within experimental uncertainty. The errors are the standard deviations over all temperatures.

Neither method is rigorous. Method 1 suffers from the fact that the linear portions of the experimental data do not extrapolate to the origin as required by the Stokes−Einstein−Smoluchowski and the Stokes−Einstein−Perrin equations. As $T/\eta \rightarrow 0$, the HSE rate constants are expected and have been found[16,41] to go to zero. Method 2 requires that the assumption that $f_{eff} = 1$ for pDT is indeed sound. We have argued elsewhere[12] that it *is* sound. Another criticism of method 2 is that, apart from the Perrin factor, the rate constants of collision of the two nitroxides are assumed to be the same. This assertion is supported by the small dependence of the HSE rate constants on probe−solvent size ratios for both probes. Despite these objections, it is encouraging that both methods are consistent with $f_{eff} = 0.49 \pm 0.03$ for CSL; i.e., HSE occurs about once every two encounters. We shall use this value in the rest of this article.

In Figure 8, we present the re-encounter rate $1/\tau_{RE}$ as a function of T/η for CSL in all three solvents and for pDT in hexane and decane together with their hydrodynamic predictions, eq 16. To find τ_{RE}, we fixed the values of Ω and k in eq 12 and fit for κ_{ER} in plots of A_{abs}/A_0 vs $\langle B\rangle/A_0$ (not shown). κ_{RE} was then used in eq 14 to calculate τ_{RE}^{HSE} and τ_{RE} followed from eq 15.[23] The re-encounter rate of pDT mostly exceeds the hydrodynamic prediction, the uppermost solid line, except in hexane at lower temperatures. The re-encounter rate of CSL in all three alkanes exceeds the hydrodynamic prediction, the lowermost solid line in Figure 8. To explore the effect of the free volume on the re-encounter rate, Figure 9 shows $1/\tau_{RE}$ for both

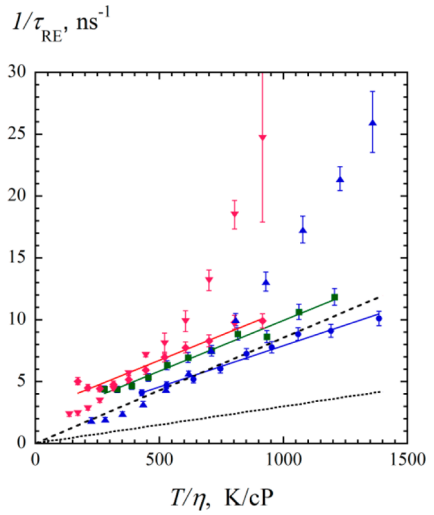

Figure 8. Re-encounter frequency versus T/η of CSL in hexane (circles), octane (squares), and decane (diamonds) and pDT in hexane (triangles) and decane (inverted triangles).[16] The solid lines are linear fits. The Stokes−Einstein prediction, eq 16, for CSL is given by the dotted line, $r_0 = 9.9$ Å, and by the dashed line for pDT, $r_0 = 7$ Å.

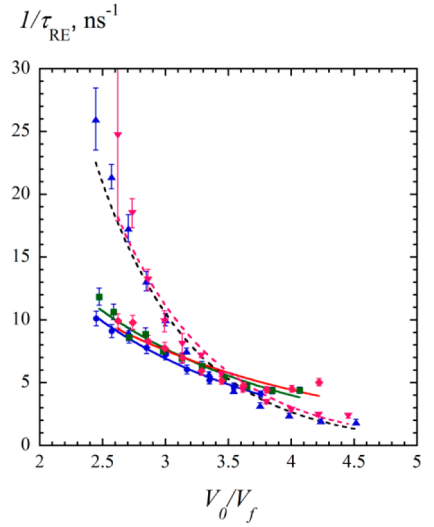

Figure 9. Re-encounter frequency versus V_0/V_f of CSL in hexane (circles), octane (squares), and decane (diamonds) and pDT in hexane (triangles) and decane (inverted triangles).[16] The solid and dashed lines are fits to eq 17.

CSL in all three solvents and pDT in hexane and decane, respectively, as functions of V_0/V_f. The curves through the data are fits to the Doolittle−Cohen−Turnbull equation. Figure 9 shows that free volume is a better predictor of the re-encounter rate than the Stokes−Einstein equation. Plots of K_{ex} vs V_0/V_f (not shown) are also well fit by the Doolittle−Cohen−Turnbull equation; however, the difference between solvents is accentuated showing that T/η is a better predictor in that case.

Values of $d\langle B_{dip}\rangle/dc = (1-\Omega)d\langle B\rangle/dc$ are shown in Figure 10 as a function of η/T and in Figure 11 as a function of V_0/V_f. The straight lines are the Stokes−Einstein equation, eq 16 of ref 41. For DD, V_0/V_f is a better predictor than T/η.

5. DISCUSSION

5.1. Strong Exchange. We have justified the use of the simplified eqs 4 and 7 for CSL based on the fact that the K_{ex}

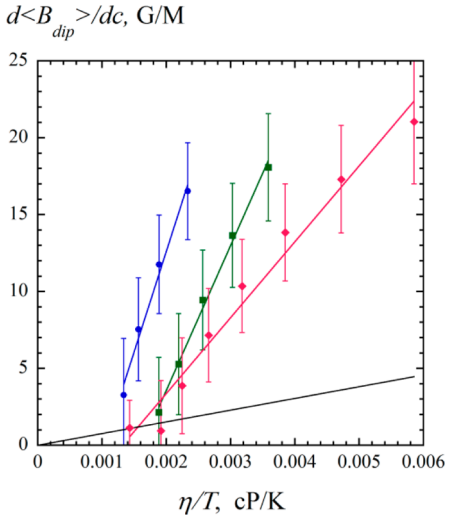

Figure 10. DD broadening rate constant of CSL vs η/T in hexane (circles), octane (squares), and decane (diamonds). The solid line is the Stokes–Einstein prediction, eq 16 from ref 41. Note that $dB_{dip}/dc \approx 49$ G/M in the static limit.[6]

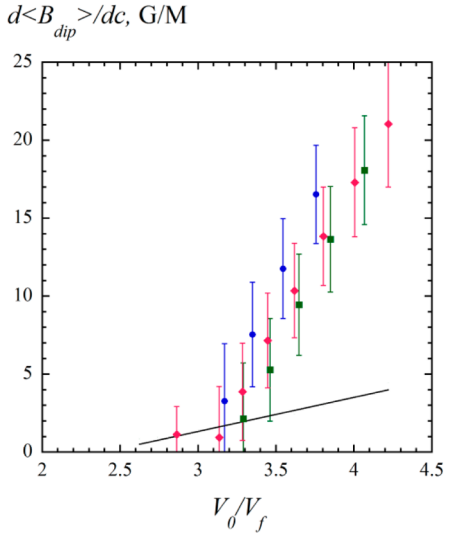

Figure 11. DD broadening rate constant of CSL vs normalized inverse free volume in hexane (circles), octane (squares), and decane (diamonds). The solid line is the Stokes–Einstein equation obtained using the relationship between V_0/V_f and η/T for decane.

is linear with T/η, Figure 7. Additional although somewhat related justification is provided by the fact that, in the case of strong exchange, the experimental values of K_{ex} must follow the Arrhenius law.[1] Plots of $\langle dB_{ex}/dc\rangle$ vs $1/T$ (not shown) for CSL show excellent agreement with the Arrhenius law with coefficients of correlation greater than 0.999 for all 3 solvents. If the $\langle dB/dc\rangle$ data are fitted to the same equation, the fits and correlation coefficients are worse, as expected.

5.2. Validity of Equation 5. Because the exchange interaction falls rapidly with interparticle separation, collisions that do not result in an overlap of the active regions are expected to occur with small values of J. There will be collisions that yield intermediate values of J, some of which lead to intermediate or weak HSE; however, these will be few because these will fall within a narrow range given by Δ, eq 20, or r_e, eq 22, both of which are small compared with the active region. Furthermore, the effect of intermediate and weak HSE on the line width is smaller and the effect on the line shifts is even smaller.[24] The fact that f_{eff} is independent of temperature supports a simple geometric interpretation. Direct support for eq 5 is provided by a comparison between the experimental $f_{eff} = 0.49 \pm 0.03$ and the theoretical $f_{eff} = 0.59 \pm 0.08$. Keeping in mind that this latter quantity is probably overestimated (see the text following eq 32), the agreement is satisfactory and shows that the inequality in eq 26 resides near the lower limit.

5.3. Diffusion of Nitroxides in Alkanes. The Stokes–Einstein equation is macroscopic, because it describes the diffusion of a large rigid spherical probe in a continuous liquid; however, bimolecular collisions are microscopic events occurring on molecular space and time scales. Therefore, it is surprising that experimental data of self-diffusion and the diffusion of solute molecules of comparable size to solvent molecules quite often follow the hydrodynamic behavior.[16,17,42] A plausible explanation for the hydrodynamic behavior of translational molecular diffusion was given by Hynes et al.[17] Using an approximate microscopic boundary condition based on conservation of momentum for the diffusion of a test hard sphere in a hard sphere solvent, they found that the diffusion coefficient is a sum of the microscopic, collisional Enskog diffusion constant and the hydrodynamic collective contribution term,[17] whose contributions are dependent on size and mass ratios of solute to solvent. The hydrodynamic collective contribution term D_h accounts for the finite solute-to-solvent size ratio and is closely related to the Stokes–Einstein diffusion constant D_{SE}[17]

$$D_h = \left(\frac{\mu}{1+\mu}\right)D_{SE} = D_{SE} - \frac{D_{SE}}{1+\mu} \tag{36}$$

where $\mu = a_p/a_s$ is the ratio of the probe radius a_p to the solvent radius a_s. When $a_p \gg a_s$, $D_h = D_{SE} = kT/4\pi a_p\eta$, that is, the Stokes–Einstein equation under slip boundary conditions.

The contributions of the Enskog term and the second term in eq 36 are opposite, and their cancellation quite well produces the Stokes–Einstein result even when the diffusion is mostly governed by microscopic events. The Hynes et al. theory[17] is not applicable at high densities for equal sized solute and solvent where backscattering caging effects are important. It is likely that the same contributions accompanied with caging effects and similar cancellations are occurring even in the high density regime, though their detailed nature is unknown.[17,43,44] Hynes et al.[17] theory has been used to explain qualitatively the translational diffusion of pDT in n-alkanes[16] and squalane.[12]

Using eq 7 to estimate f_{eff} assumes that the translational diffusion of CSL is governed by the Stokes–Einstein equation. In their paper discussing the effects of HSE and DD on the line widths of ditertiary-butyl nitroxide, Berner and Kivelson[6] argue that the discrepancy between theory and experiment for the DD component was not due to a failure of the Stokes–Einstein equation, citing work from paramagnetic relaxation enhancement NMR. In more recent work, Kowert et al. studied the translation diffusion of Buckminsterfullerene, C_{60}, in n-alkanes using microcapillary techniques and Taylor–Aris dispersion theory.[45] According to their results, the diffusion of C_{60} is slightly slower than, but within 5.5% of, the Stokes–Einstein prediction in hexane. The diffusion of C_{60} is faster than the Stokes–Einstein prediction in octane and decane where the departure from the hydrodynamic behavior increases from 3.3% in octane to 9.6% in decane. The departure from the Stokes–Einstein prediction continues increasing with the length of the n-alkane and reaches 17% in hexadecane.[45] Since the van der Waals volume of CSL,

dx.doi.org/10.1021/jp310297d | J. Phys. Chem. A 2012, 116, 12460–12469

511 Å^3, is close to the volume of C_{60}, 527 Å^3 (r = 5.01 Å),[45] it is likely that the Stokes−Einstein−Perrin equation describes the translational diffusion of CSL in hexane, octane, and decane reasonably well.

5.4. Re-Encounters of Nitroxides in Alkanes. As observed in Figure 8, the departures of τ_{RE} for pDT in alkanes from the Stokes−Einstein prediction are greater than the departures of the re-encounter rates of CSL. According to the Hynes et al. theory,[17] this result is expected; the contribution of the Enskog term, which is inversely proportional to μ, is greater for pDT because the values of μ in the case of pDT are less than those for the CSL−alkane pairs, Table 2. Note that, as the alkane length increases, in other words, μ decreases; the departures increase for both pDT and CSL re-encounter data. Therefore, the re-encounters are more dependent on the relative size of solute and solvent than the encounters, for they occur while two spin probes, enclosed in a solvent cage, are in a close proximity colliding with each other.

Table 2. Ratio of the Radii of the Spin Probe to the Solvent Molecule and Fits to eq 17

probe−solvent	$\mu = a_p/a_s$	B_{RE}[a]	r[b]	B_E[c]	r[b]
CSL−hexane	1.7	−0.71	0.992	−0.76	0.999
CSL−octane	1.5	−0.65	0.983	−0.81	0.999
CSL−decane	1.4	−0.53	0.951	−0.85	0.999
pDT−hexane	1.2	−1.37	0.995	−0.59	0.999
pDT−decane	1.0	−1.29	0.968	−0.73	0.999

[a]Re-encounters. [b]Coefficients of correlation. [c]Encounters.

5.5. Diffusion As a Function of Free Volume. Diffusion of a molecule in a liquid can be viewed as a result of redistribution of the free volume within the liquid. The diffusing molecule simply relocates into an accessible free space when it is created by a density fluctuation.[26] In this picture, the diffusion is well described by eq 17. Figures 9 and 11 demonstrate that, although the free volume is a function of temperature, the differences among the solvents for $1/\tau_{RE}$ and dB_{dip}/dc are minimized using free volume to describe their dependence on the temperature. Values of $1/\tau_{RE}$ fit the Doolittle−Cohen−Turnbull equation, eq 17, quite well. In contrast, values of K_{ex} are fit well by eq 17, but using free volume to describe the diffusion increases the discrepancy from solvent to solvent. It appears that free volume describes the short-range diffusion properties of $1/\tau_{RE}$ and $\langle dB_{dip}/dc\rangle$ while providing a poorer description of the long-range properties of K_{ex}. The values of B_{RE} and B_E, Table 2, indicate that the critical volume v^* is close to the volume V_0 of the solvent.

The fractional broadening Ω is well correlated with the Doolittle reciprocal fractional free volume V_0/V_f, Figure 6. As can be seen in Figure 6, the data for all three n-alkanes form a common curve, and the onset of DD occurs at $V_0/V_f = 3.40 \pm 0.06$. Since the re-encounter rate, $1/\tau_{RE}$, as a function of V_0/V_f also forms a common curve, we can conclude that the onset of DD in all three n-alkanes occurs at approximately $1/\tau_{RE} = 5.2$ ns^{-1}.

According to Fürth,[46] individual holes of volume V_f coalesce and form larger complex holes. Using statistical considerations, Fürth was able to calculate the mean free volume of complex holes containing n single holes, as well as the spread in their volume distribution. Positron annihilation lifetime spectroscopy is an experimental method that is well-suited for studying free volume size and volume size distribution in polymers[47,48] and ionic liquids.[49] Using positron annihilation lifetime spectroscopy, Dlubek et al.[48,49] studied the mean free volume and its spread in volume of the ionic liquid 1-methyl-3-propylimidazolium bis(trifluoromethylsulfonyl)imide as a function of temperature. They found that, at 265 K, complex holes consist of 1 to 33 single holes, or in terms of free volume, their size ranges from 20 up to 660 Å^3.[49] Also, the mean volume and spread in volume of complex holes increase with temperature. To best of our knowledge there are no positron annihilation lifetime spectroscopy measurements of free volume in neat n-alkanes, so the mean free volume and spread in volume of complex holes are not known. We believe that our results can be used to give some information of the free volume in neat n-alkanes. From the values of the onset of DD, we find that DD becomes noticeable when V_f is approximately 35 Å^3 for hexane, 57 Å^3 for octane, and 75 Å^3 for decane. Since the re-encounter rate in all three n-alkanes is the same at the onset of DD, this means that, in order to accommodate two CSL molecules (1022 Å^3), some of the complex holes have to be made of at least 30 individual holes in hexane, 18 individual holes in octane, and 14 individual holes in decane.

5.6. DD Interactions of CSL in Alkanes. When compared with other nitroxide−solvent systems, the DD onsets for CSL in n-alkanes occur at noticeably higher values of T/η. Compare the values of T/η for CSL of 640 K/cP in hexane, 450 K/cP in octane, and 400 K/cP in decane with the values of 24 K/cP (η = 13.4 cP at 317 K) for pDT in squalane and 76 K/cP (η = 4.4 cP at 337 K) for pDT in 70 wt % glycerol.[12] This difference is due to the fact that, in the case of CSL, dipole−dipole interactions are observed at much lower viscosity, that is, 0.41 cP (hexane), 0.63 cP (octane), and 0.77 cP (decane) compared with 4.4 cP (pDT in 70 wt % glycerol) and 13.4 cP (pDT in squalane). Negligible DD has been observed in the case of pDT in n-alkanes.[16] Figure 10 shows that the DD rate constant for all three alkanes is greater than the Stokes−Einstein prediction. This is opposite to the case of pDT in squalane and 70 wt % glycerol, see Figure 13 in ref 12, where the DD rate constant is below the Stokes−Einstein prediction.

6. CONCLUSIONS

The departure of K_{ex} from the Stokes−Einstein−Perrin prediction and from the results for pDT is very likely because of the steric hindrance due to the elongated shape of CSL, which is caused by an anisotropic distribution of the electron spin density. The experimental effective steric factor was evaluated by two methods, $f_{eff} = 0.49 \pm 0.03$, independent of temperature. This experimental value is in agreement with the theoretical estimate of $f = 0.35$ leading to $f_{eff} = f^{1/2} = 0.59 \pm 0.08$. Values of K_{ex} are similar in all three n-alkanes suggesting that the encounters measured by HSE are solvent independent. In contrast, the re-encounters, which occur when two spin probes are enclosed in a solvent cage, are dependent on the relative size of solute and solvent. Dipole−dipole interactions of CSL in all three solvents are observed at dramatically lower values of T/η than pDT. DD of CSL in alkanes depends on the amount of free volume in the solvent, and the threshold fractional free volume at which DD contributes to the EPR spectrum is 3.40 ± 0.06. The free volume is a better predictor of re-encounter rates; however, T/η is a somewhat better predictor of HSE.

AUTHOR INFORMATION

Corresponding Author

*E-mail: miroslav.peric@csun.edu.

Notes

The authors declare no competing financial interest.

■ ACKNOWLEDGMENTS

One of the authors (M.P.) gratefully acknowledges support from NIH Grant 1 SC3 GM099635-01.

■ REFERENCES

(1) Molin, Y. N.; Salikhov, K. M.; Zamaraev, K. I. *Spin Exchange Principles and Applications in Chemistry and Biology*; Springer: Berlin, Germany, 1980.
(2) Kivelson, D. *J. Chem. Phys.* **1960**, *33*, 1094−1106.
(3) Freed, J. H. *J. Chem. Phys.* **1966**, *45*, 3452−3453.
(4) Jones, M. T. *J. Chem. Phys.* **1963**, *38*, 2892−2895.
(5) Johnson, J. C. S. *Mol. Phys.* **1967**, *12*, 25−31.
(6) Berner, B.; Kivelson, D. *J. Phys. Chem.* **1979**, *83*, 1406−1412.
(7) Eastman, M. P.; Kooser, R. G.; Das, M. R.; Freed, J. H. *J. Chem. Phys.* **1969**, *51*, 2690−2709.
(8) Salikhov, K. M.; Doctorov, A. B.; Molin, Y. N.; Zamarev, K. I. *J. Magn. Reson.* **1971**, *5*, 189−205.
(9) Plachy, W.; Kivelson, D. *J. Chem. Phys.* **1967**, *47*, 3312−3318.
(10) Nayeem, A.; Rananavare, S. B.; Sastry, V. S. S.; Freed, J. H. *J. Chem. Phys.* **1989**, *91*, 6887−6905.
(11) Perrin, F. *J. Phys. Radium* **1936**, *7*, 1−11.
(12) Peric, M.; Bales, B. L.; Peric, M. *J. Phys. Chem. A* **2012**, *116*, 2855−2866.
(13) Galeev, R. T.; Salikhov, K. M. *Chem. Phys. Rep.* **1996**, *15*, 359−375.
(14) Salikhov, K. M. *Appl. Magn. Reson.* **2010**, *38*, 237−256.
(15) Halpern, H. J.; Peric, M.; Yu, C.; Bales, B. L. *J. Magn. Reson. A* **1993**, *103*, 13−22.
(16) Kurban, M. R.; Peric, M.; Bales, B. L. *J. Chem. Phys.* **2008**, *129*, 064501−064510.
(17) Hynes, J. T.; Kapral, R.; Weinberg, M. *J. Chem. Phys.* **1979**, *70*, 1456−1466.
(18) Dymond, J. H.; Øye, H. A. *J. Phys. Chem. Ref. Data* **1994**, *23*, 41−53.
(19) Bales, B. L.; Harris, F. L.; Peric, M.; Peric, M. *J. Phys. Chem. A* **2009**, *113*, 9295−9303.
(20) Bales, B. L.; Meyer, M.; Smith, S.; Peric, M. *J. Phys. Chem. A* **2008**, *112*, 2177−2181.
(21) Jude Jose, B.; Bales, B. L.; Peric, M. *J. Phys. Chem. B* **2009**, *113*, 13257−13262.
(22) Bales, B. L.; Peric, M. *J. Phys. Chem. A* **2002**, *106*, 4846−4854.
(23) Bales, B. L.; Peric, M.; Dragutan, I. *J. Phys. Chem. A* **2003**, *107*, 9086−9098.
(24) Salikhov, K. M. *J. Magn. Reson.* **1985**, *63*, 271−279.
(25) Doolittle, A. K. *J. Appl. Phys.* **1951**, *22*, 1471−1475.
(26) Cohen, M. H.; Turnbull, D. *J. Chem. Phys.* **1959**, *31*, 1164−1169.
(27) Berkovich, M. L.; Salikhov, K. M. *Teoret. Exp. Khim.* **1973**, *9*, 586−591.
(28) Salikhov, K. M. *Teoret. Exp. Khim.* **1974**, *10*, 310−317.
(29) Doktorov, A. B.; Yakobson, B. I. *Chem. Phys.* **1981**, *60*, 223−230.
(30) Noyes, R. M. *J. Am. Chem. Soc.* **1956**, *78*, 5488−5490.
(31) Pritchin, I. A.; Salikhov, K. M. *J. Phys. Chem.* **1985**, *89*, 5212−5217.
(32) Bales, B. L.; Mareno, B. L. D.; Harris, F. L. *J. Magn. Reson. A* **1993**, *104*, 37−53.
(33) Michon, P.; Rassat, A. *Bull. Chim. Soc. Fr.* **1971**, 3561−3567.
(34) Bondi, A. *J. Phys. Chem.* **1964**, *68*, 441−451.
(35) Zhao, Y. H.; Abraham, M. H.; Zissimos, A. M. *J. Org. Chem.* **2003**, *68*, 7368−7373.
(36) Peric, M.; Alves, M.; Bales, B. L. *Biochim. Biophys. Acta* **2005**, *1669*, 116−124.
(37) Bales, B. L.; Peric, M. *J. Phys. Chem. B* **1997**, *101*, 8707−8716.
(38) Peric, M.; Halpern, H. J. *J. Magn. Reson.* **1994**, *A 109*, 198−202.
(39) Bales, B. L.; Peric, M.; Lamy-Freund, M. T. *J. Magn. Reson.* **1998**, *132*, 279−286.
(40) Bales, B. L. In *Spin Labeling: Theory and Applications*; Berliner, J. L., Reuben, J., Eds.; Plenum: New York, 1989; Vol. *8*, pp 77−130.
(41) Bales, B. L.; Meyer, M.; Smith, S.; Peric, M. *J. Phys. Chem. A* **2009**, *113*, 4930−4940.
(42) Evans, D. F.; Tominaga, T.; Davis, H. T. *J. Chem. Phys.* **1981**, *74*, 1298−1305.
(43) Alder, B. J.; Gass, D. M.; Wainwright, T. E. *J. Chem. Phys.* **1970**, *53*, 3813−3826.
(44) Hynes, J. T. *Annu. Rev. Phys. Chem.* **1977**, *28*, 301−321.
(45) Kowert, B. A.; Dang, N. C.; Sobush, K. T.; Seel, L. G., III. *J. Phys. Chem.* **2003**, *107*, 1253−1257.
(46) Fürth, R. *Proc. Cambridge Philos. Soc.* **1941**, *37*, 252−275.
(47) Yampolskii, Y. P.; Korikov, A. P.; Shantarovich, V. P.; Nagai, K.; Freeman, B. D.; Masuda, T.; Teraguchi, M.; Kwak, G. *Macromolecules* **2001**, *44*, 4428−4438.
(48) Dlubek, G.; Hassan, E. M.; Krause-Rehberg, R.; Pionteck, J. *Phys. Rev. E* **2006**, *73* (3), 031803.
(49) Dlubek, G.; Yu, Y.; Krause-Rehberg, R.; Beichel, W.; Bulut, S.; Pogodina, N.; Krossing, I.; Friedrich, C. *J. Chem. Phys.* **2010**, *133*, 124502−124509.